Carbon segregation at Σ3 {112} grain boundaries in silicon

Dongdong Zhao, Yanjun Li*,

Department of Materials Science and Engineering, Norwegian University of Science and Technology (NTNU), 7491 Trondheim, Norway

*Corresponding author. E-mail: yanjun.li@ntnu.no Tel.: +47 73551206

Abstract

First-principles calculations were carried out to systematically investigate the carbon segregation along Σ3 {112} grain boundaries (GBs) in silicon. The energetically favorable segregation sites and corresponding segregation energy at two types of Σ3 {112} GBs, i.e. symmetric and asymmetric Σ3 {112}, were determined. A site-selective carbon segregation behavior along these two GBs was revealed, and a maximum segregation energy of -0.418 eV/atom and -0.525 eV/atom was predicted for the symmetric and asymmetric Σ3 {112} GBs, respectively. It is found that the segregation energy is linearly correlated with the average bond length (ABL) of carbon atoms segregating at the core sites in these two GBs instead of the ABL of core Si sites in the pristine Σ3 {112} GBs. Such a correlation is primarily attributed to the bonding energy effect caused by the substitution of carbon atom at the Σ3 {112} GBs, as well as the structural reconstructions of GBs along the $[1\bar{1}0]$ direction. This work provides, at the atomic level, a fundamental theoretical understanding on the carbon segregation behavior at Σ3 {112} GBs in Si.

Keywords: Carbon gettering, Σ3 {112} grain boundaries, segregation, mc-Si, first-principles calculations.

1. Introduction

Metallurgical multi-crystalline Si (mc-Si) is extensively used as the raw materials for photovoltaic Si-based solar cells with the aim to reduce production cost [1-5]. However, this type of mc-Si usually contains a large amount of various defects, e.g. grain boundaries (GBs), dislocations, etc., which are detrimental to the electrical performance of solar cells [6-9]. For instance, it is established that GBs can act as recombination centers and lead to electrical efficiency loss in mc-Si [6, 7]. As an inevitable defect in mc-Si, GBs can also act as gettering centers for impurity elements [1-4, 10-16]. The various impurities gettered along GBs can alter the recombination rates of the GB and thus exert a significant influence on the solar cell conversion efficiency [2, 4, 11, 14-16]. As one of the major impurity elements in mc-Si, carbon (C) usually stems from the casting furnace and crucible during casting and solidification process. The impact of C impurity on the property of mc-Si is complex and has long remained a research topic [17]. Pizzini et al. [10, 18] reported that the electrical activity of dislocations and GBs was exclusively controlled by the ratio of O (oxygen) to C concentration and hence dominated the minority carrier properties of mc-Si. A high level C content in mc-Si is considered to remarkably promote O precipitation [19], which can act as recombination centers, and thus is detrimental to the mc-Si based solar cell performance [4]. On basis of the research from Ref. [17, 20-22], C impurity, in an implanted state, can serve as efficient gettering centers for harmful metallic impurities, i.e. Cu, Au, Fe, etc. Recently, Stoffers et al. [2], using 3D atom probe tomography (APT) measurement and electron-beam-induced current (EBIC), precisely determined that C solutes have a strong inclination to segregate to GBs in mc-Si. These agglomerated C impurities along the GBs would play a dominant role in affecting the recombination rate of the GBs, and hence influence the minority carrier properties of mc-Si. Consequently, an in-depth understanding of C gettering behavior along GBs in mc-Si is crucial for fabrication of effective and high-performance mc-Si based solar cells.

So far, most of the research work has been focused on the gettering of detrimental metal impurities, like Fe, Cu, Ni, etc. at Si GBs [2, 3, 12-16], aiming to investigate their effects on carrier recombination and cell efficiency. Less effort has been put on the gettering behavior of C solutes along GBs in mc-Si. In a previous work, we have investigated the C gettering behavior along twin

boundaries (TBs) of Σ3, Σ9 and Σ27 in mc-Si [23]. It was found that a linear correlation between the C segregation energy at TBs and the average bond length (ABL) of the atomic sites exists. Nevertheless, the specific interactions between C solutes and other GBs remain unclear. Thereby, further calculations are needed to gain insight into the C gettering behavior along different GBs in mc-Si.

The coincidence site lattice (CSL) GBs, Σ3 {112} GBs, frequently observed in mc-Si, were selected as the GB candidates to probe the C-GB interactions. As incoherent CSL GB in Si, Σ3 {112} has been extensively investigated in the last decades [24-29]. Following the high resolution transmission electron microscopy (HRTEM) work from Sakaguchi et al. [28] and Sawada et al. [26], two variant structure models exist for Σ3 {112} GBs in Si, namely, the symmetric (S) (cf. Fig. 1(b)) and asymmetric (A) (cf. Fig. 1(c)) ones. S-Σ3 {112} GB, with a symmetrical rigid geometrical model, contains five- and seven-fold Si rings, which constitutes the dislocation core. On the contrary, A-Σ3 {112} GB undergoes rigid body displacement along the [111], [112] directions and structural reconstruction. The core structure of this GB is composed of periodic five-, seven- and six-fold Si rings, as shown in Fig. 1(c). Distinct GB structures can yield different GB properties. For instance, S-Σ3 {112} GB was proposed to be electrically active [27, 29], while A-Σ3 {112} GB was found to have no deep states or band tails in the fundamental gap, which indicates this GB is intrinsically electrically non-active [25].

In this paper, a systematic investigation is performed to probe the C segregation behavior along Σ3 {112} GBs in Si using first-principles calculations. In Section 2, the details of the calculation methodology and GB models are presented. Following that in Section 3, the equilibrium structures and GB energies of S- and A-Σ3 {112} GBs, as well as the interactions between C atoms and these two GBs are discussed. Finally, the conclusions are summarized in Section 4.

2. Methodology and grain boundary models

Density functional theory (DFT) as implemented in the Vienna ab initio simulation package (VASP) [30] was employed to perform the calculations in the present work. The frozen-core projected augmented wave (PAW) method [31, 32] was adopted for the core region and the exchange–

correlation functions were treated with the Generalized Gradient Approximation (GGA) of Perdew–Burke–Ernzerhof (PBE) [33]. The energy cutoff for the plane-wave basis was set to 400 eV. Monkhorst-Pack scheme [34] based *k*-point sampling together with the linear tetrahedron method including Blöchl corrections [35] was adopted for the Brillouin zone integrals.

During the calculations, bi-crystals, as shown in Fig. 1(a), containing two Σ3 {112} GBs and two micro-grains were adopted to maintain the periodic conditions. The misorientation (tilt) angle between the micro grains in these two models is 109.47°. Supercells containing 96 and 136 Si atoms were constructed for S-Σ3 {112} and A-Σ3 {112} GBs, respectively. Atomic relaxations were performed until the Hellmann-Feynman forces on all atomic sites were less than 10^{-2} eV·Å^{-1}.

3. Results and discussion

3.1 Grain boundary energy and structure

The GB energy, γ_{GB} of the two Σ3 {112} GBs is calculated by [36]:

$$\gamma_{GB} = \left(E_{SiGB}^{tot} - N_{Si}E_{Si}\right)/2A \quad (1)$$

where, E_{SiGB}^{tot} is the calculated total DFT energy of the bi-crystal supercell as displayed in Fig. 1(a), N_{Si} is the number of atoms in supercells, either 96 or 136, depending on the type of Σ3 {112} GB. E_{Si} is the energy of Si element per atom in the ground-state diamond phase. A is the cross-section area of the GBs. Scaling factor ½ in Eq. (1) indicates that there are two GBs in the supercell.

The relaxed ground-state atomic structures of the two Σ3 {112} GBs are consistent with the experimental observations [26, 28, 37] and theoretical calculations [15, 27, 28]. No dangling bond exists for the Si atoms in the GBs. All the Si sites in the GBs are four-fold coordinated except for site 5 in S-Σ3 {112} GB, which is five-fold coordinated as a result of rebonding between site 5 and 5′ (bond length 2.8935 Å). This extra bond can lead to deep levels in the bandgap of total density of states of S-Σ3 {112} GB, as evidenced in Ref. [29]. The calculated GB energies γ_{GB} i.e. 0.658 and 0.363 J/m^2 for S- and A-Σ3 {112} GBs, respectively (cf. Table 1), are in good agreement with the previous calculation data [15, 28, 38]. Note that A-Σ3 {112} GB has a lower γ_{GB} than S-Σ3 {112} GB, which is attributed to the structural asymmetric reconstruction of the GB. A-Σ3 {112} GB has periodically localized compression and tension areas along the GB, which is in accordance with the

five- and seven-fold rings in the GB core region. For instance, site 7 in the five-fold ring possesses a small ABL of 2.3343 Å, while site 9 in the seven-fold ring has an ABL of 2.4276 Å. In comparison to the Si-Si bond length in bulk (2.3679 Å), these two sites refer to a compression and a tension state, respectively.

Both GBs undergo structural reconstruction during atomic relaxation. Rebonding between three-fold coordinated Si core sites in the GBs occurs. As can be seen in Fig. 2, Si-Si dimer with a bond length of 2.47 Å forms along the $[1\bar{1}0]$ direction after reconstruction. As a result, core site 6 in S-Σ3 {112} GB and core sites 2, 9 in A-Σ3 {112} GB become four-fold coordinated without dangling bonds. This reconstruction of GB structure can lower the γ_{GB} and eliminate the deep levels in partial density of states, which is in agreement with earlier theoretical works [15, 28, 29].

The layer-by-layer atomic bond length and bond angle distributions of S-Σ3 {112} and A-Σ3 {112} GBs are displayed in Fig. 3(a-d), where d_e is the equilibrium bond length, i.e. 2.3679 Å, and θ_0 is the equilibrium bond angle, i.e. 109.47°, in bulk-Si. The layer numbers are as indicated in Fig. 1 (b) and (c), with each layer containing four Si atoms. The bond length and bond angle are collected according to the atomic sites in layers shown in Fig. 1(b) and (c). As indicated in Fig. 3(a) and (b), deviations in terms of bond length and bond angle from bulk-Si are characterized as $(d-d_e)/d_e$ and $\theta-\theta_0$, respectively. Larger deviations are usually observed in the vicinity of Σ3 {112} GBs (cf. Fig. 3). One can further find that this deviation either in bond length or bond angle covers more atomic layers in A-Σ3 {112} than S-Σ3 {112} GB supercells, which may be ascribed to the intrinsically asymmetric atomic structure of A-Σ3 {112} GB. In Fig. 3(a) and (b), straight lines are plotted as guidance to the eye for indication of layers with bond length deviating less than 1.5% from bulk Si. As discussed in Ref. [39], such a distortion will not cause significant energy variation. Analogously, ±10° lines are added in Fig. 3(c) and (d) to indicate the atomic layers where large bond angle distortion can happen. As shown in Fig. 3(a) and (c), the bond length and bond angle deviations of S-Σ3 {112} GB lie in the range of -1.7% to 6.4% and -40.5° to 17.4°, respectively. Layer 1 is predicted to have the largest lattice distortions, corresponding to the biggest deviations in both bond length and bond angle (cf. Fig. 1(a) and (c)). In contrast, smaller bond length and bond angle deviations ranging

from -2.2% to 4.8% and -15.4 to 16.4° were observed for A-Σ3 {112} GB, respectively, which are correlated with the lower γ_{GB} and relatively high stability of this GB. No significant lattice distortions can be observed after the 3rd and 8th atomic layer in S-Σ3 {112} and A-Σ3 {112} GB supercells, respectively, indicating that the size of the bi-crystal supercell utilized in the present work is large enough to describe the Σ3 {112} GBs.

3.2 Carbon segregation at Σ3 {112} GBs

To gain insight into the C segregation behavior along Σ3 {112} GBs, single C impurity can be inserted into the equilibrium GBs to substitute Si atoms in the core sites to evaluate the segregation energy γ_{seg} of C solutes at these two Σ3 {112} GBs [40, 41].

$$\gamma_{seg} = E_{ie}^{GB} - E_{ie}^{Bulk} \quad (2)$$

Where E_{ie}^{GB} is the impurity energy of C atom residing at the GBs, E_{ie}^{Bulk} corresponds to the impurity energy of C in bulk Si (diamond phase).

$$E_{ie}^{GB} = E_{GB}^{Si_{n-1}C} - E_{GB}^{Si_{n-1}} - \mu_C \quad (3)$$

$$E_{ie}^{Bulk} = E_{Bulk}^{Si_{n-1}C} - E_{Bulk}^{Si_{n-1}} - \mu_C \quad (4)$$

$E_{GB}^{Si_{n-1}C}$, $E_{Bulk}^{Si_{n-1}C}$ are the total DFT energy of the bi-crystal and bulk simulation supercell containing one C impurity atom, respectively; $E_{GB}^{Si_{n-1}}$, $E_{Bulk}^{Si_{n-1}}$ stand for the total energy of pristine GB simulation supercell and pure Si bulk without C impurities, respectively; and μ_C is the chemical potential of C impurity, taken as the values from the *graphite* phase. A negative γ_{seg} indicates that the C solutes prefer to segregate to the GBs from bulk environment.

The C segregation energy at different core sites along symmetric and asymmetric Σ3 {112} GBs were collected in Table 2 and displayed in Fig. 4. Apparently, the C segregation behavior along S-Σ3 {112} GB is heterogeneous and site-specific. As can be seen, S-Σ3 {112} GB has six core sites for possible C segregation (cf. Fig. 1(b)), among which, two sites (site 4, 5) exhibit negative γ_{seg}, i.e. -0.210 and -0.418 eV/atom (cf. Table 2 and Fig. 4), respectively, indicating an attractive interaction with C atoms. All the other sites are energetically unfavorable for C segregation as a result of the calculated positive γ_{seg}. Sites 4′, 5′ (cf. Fig. 1(b)) have the same value of γ_{seg} with sites 4, 5 due to the

intrinsic symmetry of the GB. The values of γ_{seg} signify that C gettering can happen along S-Σ3 {112} GBs in Si.

Similar to S-Σ3 {112} GB, a site-selective C segregation behavior along A-Σ3 {112} GB was also predicted. However, the interactions between C atoms and A-Σ3 {112} GB are more complex. As indicated in Fig. 1(c), there are 16 distinct substitutional core sites for possible C segregation along A-Σ3 {112} GB. Five sites were calculated in this work to possess a negative γ_{seg} (cf. Table 2 and Fig. 4), whereas site 7, as the joint site of five-fold and two six-fold rings, was predicted to have the most negative γ_{seg}, i.e. -0.525 eV/atom, which is even lower than the segregation energy of site 5, 5′ in S-Σ3 {112} GB. This behavior is analogous to the C segregation in Σ27 {552} TB in Si, as studied in a previous work [23], in which the joint site of five-fold and two six-fold rings was predicted to be the most attractive for C segregation. The utmost positive γ_{seg}, i.e. 0.818 eV/atom, in A-Σ3 {112} GB is higher than that in S-Σ3 {112} GB, corresponding to the stronger repulsive interaction (cf. Table 2 and Fig. 4). Furthermore, A-Σ3 {112} GB is considered to exhibit a higher ability to getter C atoms than S-Σ3 {112} GB, due to the more energetically favorable sites and more negative γ_{seg} for C segregation (cf. Table 2 and Fig. 4).

In a previous work [23], it was revealed that the intrinsic lattice distortion (mainly bond length deviation) in the TBs in mc-Si is the main driving force for the C gettering, where core sites with a smaller ABL in the TBs exhibit a higher propensity for C segregation. A linear correlation was demonstrated between the atomic-site specific segregation energy for C at TBs and the ABL of atomic sites [23]. An attempt is also made to correlate the segregation energy of C and the geometrical character of the segregation sites (including ABL, bond angle, etc.) in the pristine Σ3 {112} GBs. The γ_{seg} values of all core sites are plotted in Fig. 5(a) as a function of ABL of the core Si sites in the pristine GBs. Unfortunately, the data points are scattering and do not follow the linear correlation between the γ_{seg} for C at TBs and the ABL of atomic sites as documented in Ref. [23]. This can be ascribed to the structure reconstruction along the $[1\bar{1}0]$ direction, in which the re-bonding between

three-fold coordinated Si atoms can introduce more lattice deviation both in bond length and bond angle, in comparison to the CSL TBs previously studied [23].

Fig. 5(b) shows the segregation energy as a function of the ABL of each C atomic site (the Si atoms at each core site of the Σ3 {112} GBs is replaced by a C atom). Interestingly, most of the data again show a general trend that γ_{seg} increases with ABL and a linear correlation can be fitted, i.e.,

$$\gamma_{seg}=18.6901\cdot(\mathrm{ABL}-2.0114) \quad (5)$$

This correlation can be partially accounted for with the C-Si bonding energy effect of the GB sites with C segregation. As discussed in a previous work [23], C atoms always turn to form shorter covalent bonds with surrounding Si host atoms than the Si-Si bonds. A short C-Si bond length would represent a high bonding energy state. For instance, β-SiC possesses the most stable C-Si bond with a bond length of 1.8878 Å, which corresponds to the highest bonding energy [42]. As evidenced by the present calculations, substitutional C atoms can lead to a severe lattice contraction of Si bulk crystal, as a result of the formation of short C-Si covalent bonds (bond length 2.0194 Å, cf. Fig. 6(a)). In this work, site 7 in A-Σ3 {112} GB is predicted to be the most energetically favorable site for C segregation, which is attributed to the short ABL of the site. As indicated in Fig. 6(b), when site 7 in A-Σ3 {112} GB is replaced by a C atom, an ABL of 1.9785 Å (Fig. 6(b)) can be achieved, which is smaller than the length of substitutional C-Si covalent bonds (2.0194Å) in bulk Si environment as depicted in Fig. 6(a). This shorter ABL refers to a higher bonding energy state and therefore a low total DFT energy of the simulation supercell. The bonding energy penalty from the C-Si bonds at Si GB in reference to that in the bulk environment is considered to be the main reason for the strong attractive interaction between C atom and site 7 in A-Σ3 {112} GB. Furthermore, as discussed in a former part, site 7 is located at the compressive region (five-fold ring) along the pristine A-Σ3 {112} GB, subjected to a compression strain field. The segregation of smaller C solute at site 7 is energetically favorable since it can release the localized residual stress and thus decrease the compressive elastic strain energy of the GB. So, in addition to the bonding energy, the intrinsic lattice distortion also contributes to the C segregation at site 7 in A-Σ3 {112} GB.

However, there is one core site, namely site 5 in S-Σ3 {112} GB, deviating far from the linear correlation shown in Fig. 6(b). Site 5 is calculated to be the most attractive site for C segregation in S-Σ3 {112} GB. Surprisingly, as shown in Fig. 5, the values of γ_{seg} and the ABL for this site is deviating far from linear trend line depicted by Eq. (5). As indicated in Fig. 6(c), the four C-Si covalent bonds exhibit a ABL of 1.9507 Å, which is even smaller than the ABL of site 7 in A-Σ3 {112} GB with C segregation, contributing significantly to the negative γ_{seg} of C segregation. However, due to the intrinsic symmetry of S-Σ3 {112} GB, site 5 does not possess a more negative γ_{seg} than site 7 in A-Σ3 {112} GB. It can be seen from Fig. 6(c) that Si atom at site 5′ is close to the C impurity, with a distance of 2.9254 Å, being 155.0% of the C-Si bond length in β-SiC [42]. The C-Si bond is considered weak and in a low bonding energy state, which would raise the total system energy and γ_{seg} for C segregation, accounting for the deviation of γ_{seg} and the ABL of site 5 from the linear relationship of Eq. (5).

4. Conclusion

In the present work, the C segregation behaviors along Σ3 {112} GBs in silicon have been systematically investigated via first-principles calculations. It is found that the site-selective C segregation can both occur along S-Σ3 {112} (symmetric) and A-Σ3 {112} (asymmetric) GBs, wherein A-Σ3 {112} exhibits a stronger C-GB interaction energy, as well as a higher C gettering ability. Due to the structural reconstruction effect of the GBs, the segregation energy of C in Σ3 {112} GBs does not follow the linear correlation with the ABL of Si atomic core sites (Si-Si bond) in the GBs. Instead it is linearly related with the ABL of C atoms (C-Si bonds) segregating at the cores sites at these two GBs, which is ascribed to the bonding energy effect caused by the substitution of C atoms. The present work can provide fundamental knowledge upon the interactions between C impurities and Σ3 {112} GBs in mc-Si at the atomic level, which is essential and important for photovoltaic applications of mc-Si to design high-performance solar cells.

Acknowledgement

This work is financially supported under the FRINATEK project 'BENTMAT' (project number 222173) from the Research Council of Norway. Computation time from the NOTUR consortium is gratefully acknowledged.

References

[1] P. Käshammer, T. Sinno, Interactions of twin boundaries with intrinsic point defects and carbon in silicon, J. Appl. Phys., 114 (2013) 083505.

[2] A. Stoffers, O. Cojocaru-Mirédin, W. Seifert, S. Zaefferer, S. Riepe, D. Raabe, Grain boundary segregation in multicrystalline silicon: correlative characterization by EBSD, EBIC, and atom probe tomography, Prog. Photovolt: Res. Appl., 23 (2015) 1742–1753.

[3] P. Käshammer, T. Sinno, A mechanistic study of impurity segregation at silicon grain boundaries, J. Appl. Phys., 118 (2015) 095301.

[4] Y. Ohno, K. Inoue, K. Fujiwara, M. Deura, K. Kutsukake, I. Yonenaga, Y. Shimizu, K. Inoue, N. Ebisawa, Y. Nagai, Three-dimensional evaluation of gettering ability for oxygen atoms at small-angle tilt boundaries in Czochralski-grown silicon crystals, Appl. Phys. Lett., 106 (2015) 251603.

[5] S. Ratanaphan, Y. Yoon, G.S. Rohrer, The five parameter grain boundary character distribution of polycrystalline silicon, J. Mater. Sci., 49 (2014) 4938–4945.

[6] J. Chen, T. Sekiguchi, D. Yang, F. Yin, K. Kido, S. Tsurekawa, Electron-beam-induced current study of grain boundaries in multicrystalline silicon, J. Appl. Phys., 96 (2004) 5490-5495.

[7] H.Y. Wang, N. Usami, K. Fujiwara, K. Kutsukake, K. Nakajima, Microstructures of Si multicrystals and their impact on minority carrier diffusion length, Acta Mater., 57 (2009) 3268–3276.

[8] A. Stoffers, B. Ziebarth, J. Barthel, O. Cojocaru-Mirédin, C. Elsässer, D. Raabe, Complex Nanotwin Substructure of an Asymmetric Σ9 Tilt Grain Boundary in a Silicon Polycrystal, Phys. Rev. Lett., 115 (2015) 235502.

[9] V.Y. Lazebnykh, A.S. Mysovsky, Ab initio and atomistic simulation of local structure and defect segregation on the tilt grain boundaries in silicon, J. Appl. Phys., 118 (2015) 135704.

[10] S. Pizzini, P. Cagnoni, A. Sandrinelli, M. Anderle, R. Canteri, Grain boundary segregation of oxygen and carbon in polycrystalline silicon, Appl. Phys. Lett., 51 (1987) 676-678.

[11] T. Buonassisi, A.A. Istratov, M.D. Pickett, M. Heuer, J.P. Kalejs, G. Hahn, M.A. Marcus, B. Lai, Z. Cai, S.M. Heald, T.F. Ciszek, R.F. Clark, D.W. Cunningham, A.M. Gabor, R. Jonczyk, S. Narayanan, E. Sauar, E.R. Weber, Chemical Natures and Distributions of Metal Impurities in Multicrystalline Silicon Materials, Prog. Photovolt: Res. Appl., 14 (2006) 513–531.

[12] T.T. Shi, Y.H. Li, Z.Q. Ma, G. H. Qu, F. Hong, F. Xu, Y.F Yan, S.-H. Wei, First-principles study of iron segregation into silicon Σ5 grain boundary, J. Appl. Phys., 107 (2010) 093713.

[13] A. Autruffe, L. Vines, L. Arnberg, M.D. Sabatino, Impact of growth rate on impurities segregation at grain boundaries in silicon during Bridgman growth, J. Crys. Growth., 372 (2013) 180–188.

[14] A. Autruffe, L. Arnberg, M.D. Sabatino, Coincident site lattice bi-crystals growth—Impurity segregation towards grain boundaries, J. Cryst. Growth., (2015) 8-11.

[15] B. Ziebarth, M. Mrovec, C. Elsässer, P. Gumbsch, Interstitial iron impurities at grain boundaries in silicon: A first-principles study, Phys. Rev. B, 91 (2015) 035309.

[16] B. Chen, J. Chen, T. Sekiguchi, M. Saito, K. Kimoto, Structural characterization and iron detection at Σ3 grain boundaries in multicrystalline silicon, J. Appl. Phys., 105 (2009) 113502.

[17] W. Skorupa, R.A. Yankov, Carbon-mediated effects in silicon and in silicon-related materials, Materials Chemistry and Physics, 44 (1996) 101-144.

[18] S. Pizzini, A. Sandrinelli, M. Beghi, D. Narducci, F. Allegretti, S. Torchio, G. Fabbri, G.P. Ottaviani, F. Demartin, A. Fusi, Influence of Extended Defects and Native Impurities on the Electrical Properties of Directionally Solidified Polycrystalline Silicon, J. Electrochem. Soc., 135 (1988) 155-165.

[19] B. Gao, X.J. Chen, S. Nakano, K. Kakimoto, Crystal growth of high-purity multicrystalline silicon using a unidirectional solidification furnace for solar cells, J. Crys. Growth., 312 (2010) 1572–1576.

[20] H. Wong, N.W. Cheung, K.M. Yu, P.K Chu, J. Liu, Impurity Gettering by Implanted Carbon in Silicon, Mat. Res. Soc. Symp. Proc., 147 (1989) 97-106.

[21] H. Wong, N.W. Cheung, P.K. Chu, Gettering of gold and copper with implanted carbon in silicon, Appl. Phys. Lett., 52 (1988) 889-891.

[22] W. Skorupa, N. Hatzopoulos, R.A. Yankov, A.B. Danilin, Proximity gettering of transition metals in separation by implanted oxygen structures, Appl. Phys. Lett., 67 (1995) 2992-2994.

[23] D.D. Zhao, Y.J. Li, Lattice distortion induced site dependent carbon gettering at twin boundaries in silicon, J. Alloys. Comp., 712 (2017) 599-604.

[24] C. Fontaine, D.A. Smith, On the atomic structure of the Σ3 {112} twin in silicon, Appl. Phys. Lett., 40 (1981) 153-154.

[25] M. Kohyama, R. Yamamoto, Y. Watanabe, Y. Ebata, M. Kinoshita, The atomic and electronic structure of the Σ=3 (211) twin boundary in Si, J. Phys. C: Solid State Phys., 21 (1988) L695-L700.

[26] H. Sawada, H. Ichinose, Structure of {112} Σ3 boundary in Silicon and Diamond, Scr. Mater., 44 (2001) 2327–2330.

[27] H. Sawada, H. Ichinose, M. Kohyama, Gap states due to stretched bonds at the (112) Σ3 boundary in diamond, J. Phys.: Condens. Matter, 19 (2007) 026223.

[28] N. Sakaguchi, H. Ichinose, S. Watanabe, Atomic Structure of Faceted Σ3 CSL Grain Boundary in Silicon: HRTEM and Ab-initio Calculation, Mater. Trans., 48 (2007) 2585-2589.

[29] C.B. Feng, J.L. Nie, X.T. Zu, M.M. Al-Jassim, Y.F. Yan, Structure and effects of vacancies in Σ3 (112) grain boundaries in Si, J. Appl. Phys., 106 (2009) 113506.
[30] G. Kresse, J. Furthmüller, Efficient iterative schemes for ab initio total-energy calculations using a plane-wave basis set, Phys. Rev. B, 54 (1996) 11169-11186.
[31] P.E. Blöchl, Projector augmented-wave method, Phys. Rev. B, 50 (1994) 17953-17979.
[32] G. Kresse, D. Joubert, From ultrasoft pseudopotentials to the projector augmented-wave method, Phys. Rev. B, 59 (1999) 1758-1775.
[33] J.P. Perdew, K. Burke, M. Ernzerhof, Generalized Gradient Approximation Made Simple, Phys. Rev. Lett., 77 (1996) 3865.
[34] H.J. Monkhorst, J.D. Pack, Special points for Brillouin-zone integrations, Phys. Rev. B, 13 (1976) 5188-5192.
[35] P.E. Blöchl, O. Jepsen, O.K. Andersen, Improved tetrahedron method for Brillouin-zone integrations, Phys. Rev. B, 49 (1994) 16223-16233
[36] J. Xu, Y. Jiang, L.T. Yang, J.X. Li, Assessment of the CSL and SU models for bcc-Fe grain boundaries from first principles, Comp. Mater. Sci., 122 (2016) 22-29.
[37] H. Sawada, H. Ichinose, M. Kohyama, Atomic structure of the Σ3 and Σ9 grain boundaries in CVD diamond film, Scr. Mater., 51 (2004) 689–692.
[38] Y.-H. Li, S.-K. Guo, Z.-Q. Ma, G.-H. Qu, T.-T. Shi, X.-G. Gong, Q. Xia, S.-H. Wei, Magnetic property of transition metal-Si atomic line on silicon Σ3 grain boundary: A theoretical study, J. Appl. Phys., 115 (2014) 223906.
[39] W.L. Huang, W. Ge, C.X. Li, C.F. Hou, X.W. Wang, X.F. He, Atomic and electronic structures of Si[001] (130) symmetric tilt grain boundaries based on first-principles calculations, Comp. Mater. Sci., 58 (2012) 38-44.
[40] W.G. Liu, H. Han, C.L. Ren, H.Q. Yin, Y. Zou, P. Huai, H.J. Xu, Effects of rare-earth on the cohesion of Ni Σ5 (012) grain boundary from first-principles calculations, Comp. Mater. Sci., 96 (2015) 374-378.
[41] Y.P. Li, C. Han, C.L Zhang, K. Jia, P.D Han, X.L. Wu, Effects of alloying on the behavior of B and S at Σ5 (210) grain boundary in γ-Fe, Comp. Mater. Sci., 115 (2016) 170-176.
[42] J. Dong, A.-B. Chen, Fundamental Properties of SiC: Crystal Structure, Bonding Energy, Band Structure, and Lattice Vibrations, Springer, 2004.

Tables

Table 1. Grain boundary energy, γ_{GB}, of symmetric S-Σ3 {112} and asymmetric A-Σ3 {112} GBs. The previous theoretical data in the literature are also included for comparison.

Grain boundary	Misorientation angle, θ	Grain boundary energy, γ_{GB}, J/m^2			
		This work (DFT)	[a]Ziebarth	[b]Sakaguchi	[c]Li
S-Σ3 {112}	109.47°	0.658	0.67	0.76	-
A-Σ3 {112}	109.47°	0.363	0.47	0.56	0.40

[a]from Ref. [15].

[b]from Ref. [28].

[c]from Ref. [38].

Table 2. Carbon segregation energy at different core sites along symmetric S-Σ3 {112} and asymmetric A-Σ3 {112} GBs. The energy is in eV/atom. The core sites for carbon segregation are indicated with numbers in Fig. 1.

Grain boundary	Core sites	Segregation energy, eV/atom	Grain boundary	Core sites	Segregation energy, eV/atom
S-Σ3 {112}	1	0.763	A-Σ3 {112}	6	-0.072
	2	0.149		7	-0.525
	3	0.116		8	-0.090
	4	-0.210		9	0.818
	5	-0.418		10	0.368
	6	0.606		11	0.043
A-Σ3 {112}	1	0.001		12	-0.207
	2	0.483		13	0.002
	3	0.430		14	-0.060
	4	0.583		15	0.407
	5	0.174		16	0.373

Figures

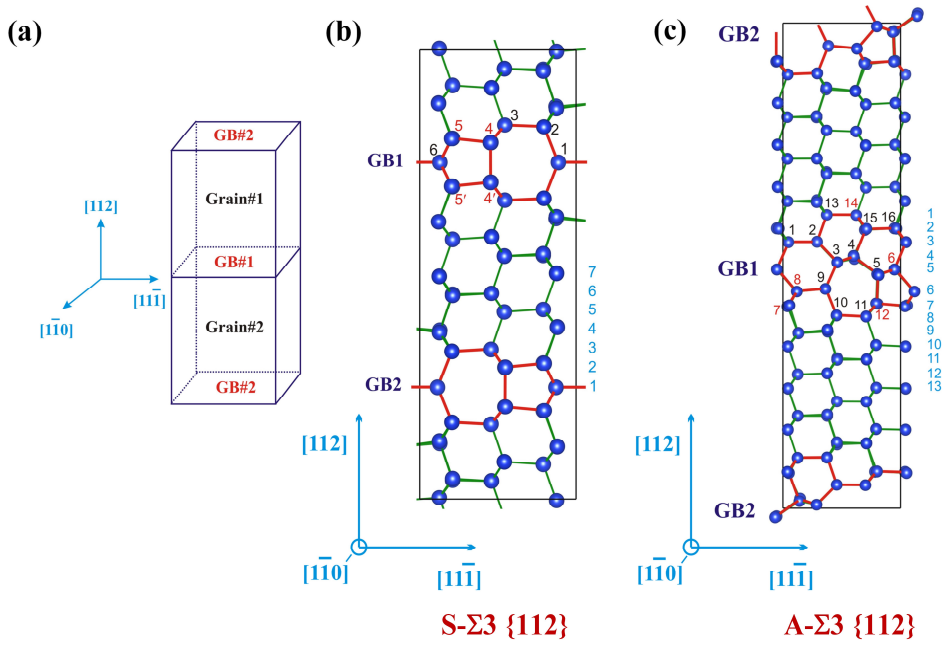

Fig. 1. (a) Sketch of bi-crystal structure used in the present work. Structures of symmetric (b) S-Σ3 {112} and asymmetric (c) A-Σ3 {112} GBs as projected in the $<1\bar{1}0>$ direction. The core sites of the two grain boundaries for carbon segregation are marked out with numbers. The red numbers indicate energetically favorable carbon segregation.

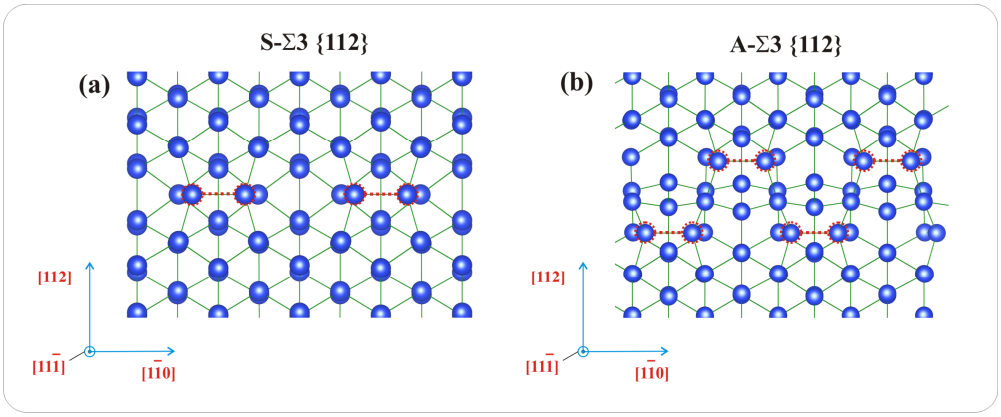

Fig. 2. Reconstruction of Si atomic bonds in symmetric (a) S-Σ3 {112} and asymmetric (b) A-Σ3 {112} GBs along the [1$\bar{1}$0] direction. Si-Si dimers are marked out.

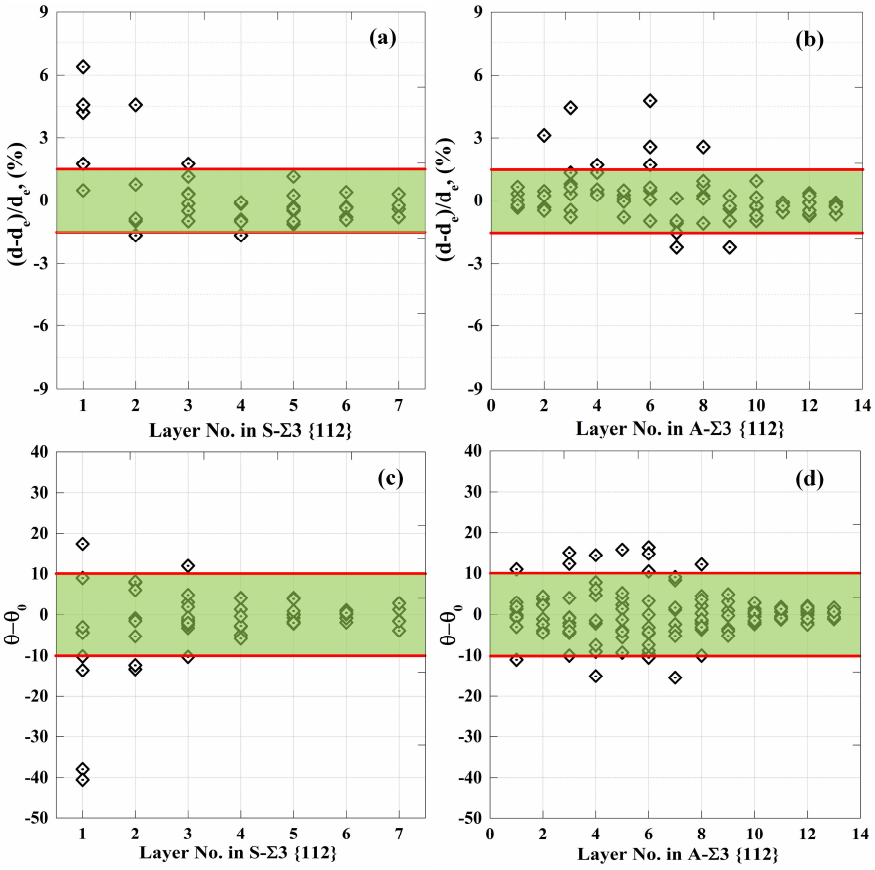

Fig. 3. The layer-by-layer Si-Si bond length and bond angle distributions of symmetric (a, c) S-Σ3 {112} and asymmetric (b, d) A-Σ3 {112} GBs. The layer numbers are as indicated in Fig. 1(b) and (c). d_e is the equilibrium bond length, i.e. 2.3679 Å, and θ_0 is the bond angle, i.e. 109.47°, in bulk-Si.

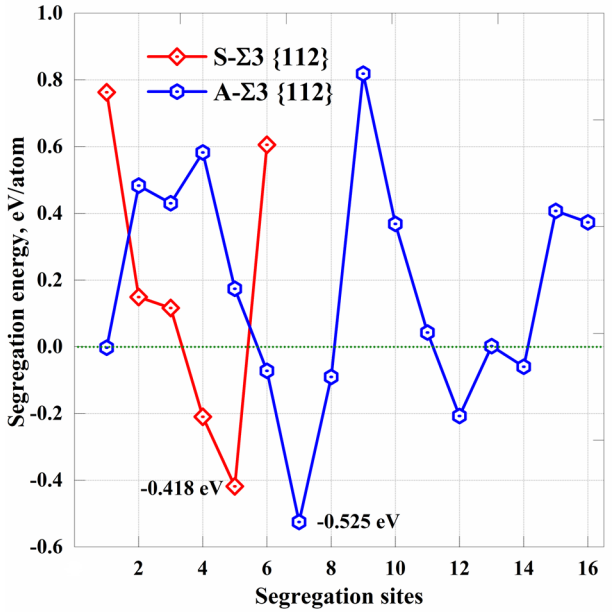

Fig. 4. Segregation energy of carbon atoms at each core site of symmetric S-Σ3 {112} and asymmetric A-Σ3 {112} GBs. The energy unit is in eV/atom. The segregation sites for each GB are as indicated in Fig. 1.

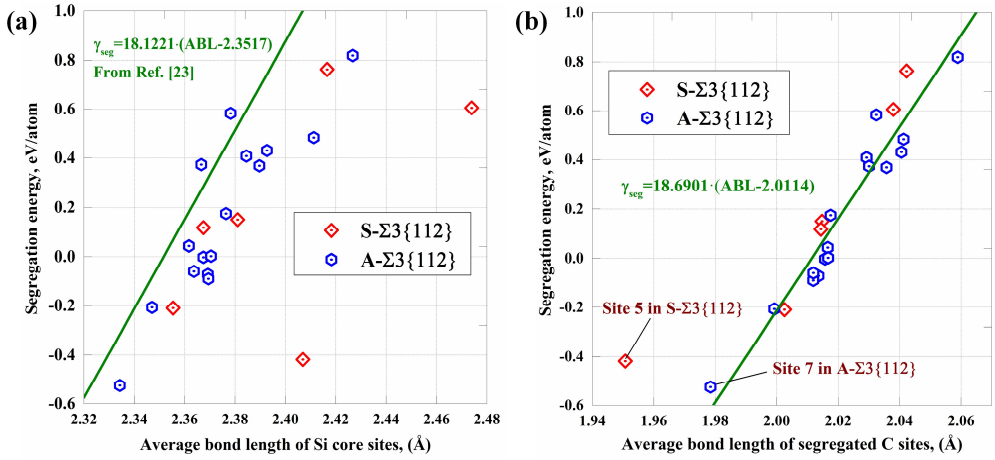

Fig. 5. (a) Carbon segregation energy as a function of average bond length (ABL) of the Si core sites in the pristine symmetric S-Σ3 {112} and asymmetric A-Σ3 {112} GBs, the linear correlation in Ref. [23] is also included for comparison. (b) Carbon segregation energy as a function of average bond length (ABL) of the segregated C sites at symmetric S-Σ3 {112} and asymmetric A-Σ3 {112} GBs. The energy is in eV/atom.

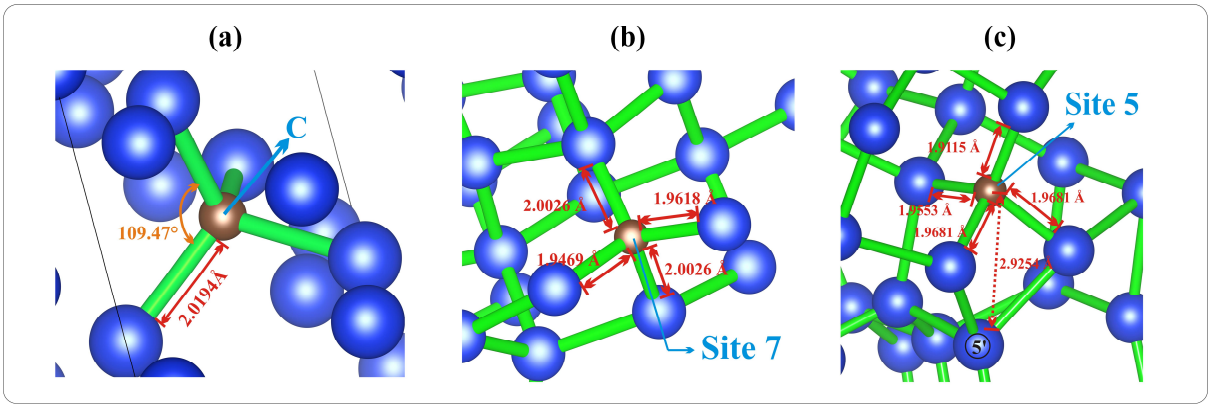

Fig. 6. (a) Bonding environment of substitutional C atom in bulk Si. (b) Bonding environment of substitutional C atom at core site 7 along asymmetric A-Σ3 {112} GB. (c) Bonding environment of substitutional C atom at core site 5 along symmetric S-Σ3 {112} GB.